Ab Initio Calculation of the Electron Density of Tetraazatetraoxatricyclotetradecane: An Explanation for the Deficiency of Charge Density in Certain Covalent Bonds†

Kathryn L. Kunze and Michael B. Hall*

Contribution from the Department of Chemistry, Texas A&M University, College Station, Texas 77843. *Received January 26, 1987*

Abstract: The standard deformation density, molecular density minus spherical atom densities, may have features, such as density deficits or weak density accumulations in covalent bonds that *seem* inconsistent with conventional chemical theory. The interpretation of these unexpected features has been controversial. Using ab initio molecular orbital methods, we are able to reproduce all of the major features in the experimental contour maps of the standard deformation density for 1,2,7,8-tetraaza-4,5,10,11-tetraoxatricyclo[6.4.1.1]tetradecane by Dunitz and Seiler (*J. Am. Chem. Soc.* **1983**, *105*, 7057-7058). In particular, maps for the O–O bond show an electron density deficit throughout the internuclear region, and density accumulations at each O in the π regions perpendicular to the O–O bond axis. Our analysis shows that these unexpected features arise because spherical atoms rather than valence-state atoms are substracted from the total density to form the deformation density. If one views bond formation in two steps, atom preparation and then bond formation, one easily sees the origin of the unexpected features in the standard deformation density. The density difference due to atom preparation (orientation of components of spherical O atom, and then promotion, polarization, and hybridization of all the atoms) is seen by subtraction of the electron densities of spherical atoms from that of optimally hybridized valence-state atoms. The density difference due to covalent bond formation (constructive interferences and charge transfer) is revealed by subtraction of the electron densities of optimally hybridized valence-state atoms from that of the molecule. The latter is dominated by a sum of two-electron bonding density differences, each of which can be isolated. For the O–O bond these reveal not only the strong accumulation of charge in the internuclear region but also the concomitant depletion of charge in the nonbonding regions which together are the signature of the covalent bond. The unexpected features arise from the O atoms preparation for bonding: orientation, promotion, and hybridization. Thus, we have used the concept of a valence-state atom to produce a useful partitioning scheme which reveals features related to chemical concepts that are not visible in the total density or in the standard deformation density and which has the potential to indicate the relative strength of various bonds.

Presently, considerable attention is being paid to studies of the electron density distribution, $\rho(r)$, in molecules. It is an observable that can be measured by experiment and predicted by theory.[1] Part of the interest arises from the promise, given by the theorem of Hohenberg and Kohn,[2] of the existence of a direct relationship between the electron density and the energy of the ground-state molecule. With improved experimental design, there is hope of obtaining essential chemical information directly from the charge distribution which is not available from other experimental methods. Most X-ray diffraction studies present what is called the standard deformation density, $\Delta\rho(r)$, which is defined as the molecular electron density minus the electron density of the promolecule[3] made up of the superposition of isolated, neutral, spherically averaged, ground-state atoms.

Recently, the X-ray crystal structure[4a-c] and the standard deformation density[4a] of 1,2,7,8-tetraaza-4,5,10,11-tetraoxatricyclo[6.4.1.1]tetradecane have been reported by Dunitz and Seiler. They were interested in the characterization of the electron density in polar and nonpolar covalent bonds[4b] and in correlating the density accumulations in the standard deformation density with the relative strengths of different kinds of covalent bonds and different kinds of lone pairs, in the same molecule. However, many features appear to be inconsistent with such a simple interpretation. For example, density deficits were found for the O-O bond and only weak density accumulations were found for the N–N, C–N, and C–O bonds.[4a] Numerous other experimental and theoretical studies[5-11] have reported standard deformation density maps which show density deficits or weak density accumulations at or near positions where "bonding density" peaks were expected between formally covalently bonded atoms. For example, electron density deficits are found in the experimental and theoretical maps of the O–O bond in H_2O_2[6,7] and theoretical maps of the F–F bond in F_2.[7] Weak electron density accumulations were found in the bonding regions in experimental maps for C–N,[1] N–N,[10] C–O,[9] N–O,[11] and C–F[5,8] bonds of various other organic molecules. Dunitz and Seiler concluded that "accumulation of charge (bonding density) in the internuclear region as occurs in the hydrogen molecule may not be characteristic of covalent bonds in general."[4a]

There is a continuing controversy over the origin of covalent bonding.[3,12-17] The prototypes for the covalent bond are the bonds

† Presented at 13th Congress and General Assembly of the International Union of Crystallography, Aug 9-18, 1984, Hamburg, FDR.

(1) Coppens, P.; Hall, M. B., Eds.; *Electron Distributions and the Chemical Bond*; Plenum Press: New York, 1982.
(2) Hohenberg, P.; Kohn, W. *Phys. Rev. B* **1964**, *136*, 864.
(3) Hirshfeld, F. L.; Rzotkiewicz, S. *Mol. Phys.* **1974**, *27*, 1319.
(4) (a) Dunitz, J. D.; Seiler, P. *J. Am. Chem. Soc.* **1983**, *105*, 7056. (b) Whittleton, S. N.; Seiler, P.; Dunitz, J. D. *Helv. Chim. Acta* **1981**, *64*, 2614. (c) Dunitz, J. D.; Schweizer, W. B.; Seiler, P. *Acta Crystallogr., Sect. A* **1981**, *37*, Suppl. C-129.
(5) (a) Dunitz, J. D.; Schweizer, W. B.; Seiler, P. *Helv. Chim. Acta* **1983**, *66*, 123. (b) Seiler, P.; Schweizer, W. B.; Dunitz, J. D. *Acta Crystallogr., Sect. B* **1984**, *40*, 319. (c) Hirshfeld, F. L. *Ibid.* **1984**, *40*, 484. (d) Hirshfeld, F. L. *Ibid.* **1984**, *40*, 613.
(6) Savariault, J. M.; Lehmann, M. S. *J. Am. Chem. Soc.* **1980**, *102*, 1298.
(7) (a) Breitenstein, M.; Dannohl, H.; Meyer, H.; Schweig, A.; Seeger, R.; Seeger, U.; Zittlau, W. *Int. Rev. Phys. Chem.* **1983**, *3*, 335. (b) Breitenstein, M.; Dannohl, H.; Meyer, H.; Schweig, A.; Zittlau, W. In ref 1.
(8) Dunitz, J. D.; Schweizer, W. B.; Seiler, P. *Helv. Chim. Acta* **1983**, *66*, 134.
(9) (a) van der Wal, H. R.; Vos, A. *Acta Crystallogr., Sect. B* **1979**, *35*, 1804. (b) Maverick, E.; Seiler, P.; Schweizer, W. B.; Dunitz, J. D. *Ibid.* **1980**, *36*, 615.
(10) (a) Hope, H.; Otterson, T. *Acta Crystallogr., Sect. B* **1979**, *35*, 370. (b) Otterson, T.; Almolf, J.; Carle, J. *Acta Chem. Scand., Ser. A* **1982**, *36*, 63. (c) Otterson, T.; Hope, H. *Acta Crystallogr., Sect. B* **1979**, *35*, 373.
(11) (a) Wang, Y.; Blessing, R. H.; Ross, F. K.; Coppens, P. *Acta Crystallogr., Sect. B* **1976**, *32*, 572. (b) Coppens, P.; Lehmann, M. S. *Ibid.* **1976**, *32*, 1777. (c) De With, G.; Harkema, S.; Feil, D. *Ibid.* **1975**, *31*, 227.
(12) (a) Ruedenberg, K. *Rev. Mod. Phys.* **1962**, *34*, 326. (b) Feinberg, M. J.; Ruedenberg, K.; Mehler, E. L. *Adv. Quantum Chem.* **1970**, *5*, 28. (c) Feinberg, M. J.; Ruedenberg, K. *J. Chem. Phys.* **1971**, *54*, 1495. (d) Kutzelnigg, W. *Angew. Chem.* **1973**, *85*, 551; *Angew. Chem., Int. Ed., Engl.* **1973**, *12*, 546. (e) Levine, I. N. *Quantum Chemistry*, 3rd ed.; Allyn and Bacon: Boston, 1983; Chapter 13.
(13) (a) Bader, R. F. W.; Chandra, A. K. *Can. J. Chem.* **1968**, *46*, 953. (b) Bader, R. F. W.; Preston, H. J. T. *Int. J. Quantum Chem.* **1969**, *3*, 327.
(14) Coulson, C. A. *Valence*, 2nd ed.; Oxford University Press: London, 1961; especially pp 81-91.

0002-7863/87/1509-7617$01.50/0

of the hydrogen molecule and hydrogen molecule ions,[12,13] where the buildup of electron density in the bonding region between the nuclei and the depletion in the nonbonding region are the signature of covalent bonding. However, the results of sophisticated theoretical calculations using atomic reference densities had lead Bader et al.[15-17] and Hirshfeld and Rzotkiewicz[3] to stress the atypical nature of the hydrogen molecule and its unsuitability for a general discussion of the covalent bond.

Hirshfeld and Rzotkiewicz[3] found for the first-row diatomics that only the hydrogen molecule is stable with respect to the spherical atom promolecule and that the accumulation in the π regions at the atoms perpendicular to the bond axis seemed more important for bonding between electronegative atoms for which the valence shells are more than half-filled. They postulated that the charge deficit in the bond region between electron-rich atoms can be attributed to the exclusion principle working against buildup in that region. Using a promolecule of properly oriented ground-state atoms, Bader et al.[15-17] found that, except for Li_2, the first-row diatomics did not fit the simple picture, but showed density accumulation in the antibinding regions which is comparable to, and in the case of F_2 exceeding, that in the binding region. H_2 and H_2^+, of course, do not exhibit a separate and significant increase in density in their antibonding region because no lone pairs are present. In addition, Feinberg and Ruedenberg showed that, in H_2^+, bonding electron density is insufficient by itself to give binding.[12c] Recently, Bader and co-workers have analyzed the total density directly by examining the Laplacian of the density.[18] However, for F_2 the Laplacian does not reveal the covalent bond.[18c,19]

Using F_2 as the simplest example, we recently showed why the accumulation of density in the standard deformation density of covalent bonds between electronegative atoms may appear weak or absent.[20] We demonstrated that the standard deformation density involving atoms with nearly filled valence shells is dominated by orientation of the components of the ground-state atom. Concurrently, Schwarz, Valtazanos, and Ruedenberg[21] published an extensive study of theoretical deformation densities for several diatomic molecules as functions of internuclear distance. They studied the effective valence potential and the decomposition of difference densities into bonding and nonbonding contributions. Also, Hirshfeld has also recently used the stockholder decomposition to define nonspherical atomic orbital fragments.[22] In our analysis of F_2 we also used a valence-state atom to produce a partitioning scheme which reveals not only the strong accumulation of charge in the internuclear region but also the concomitant depletion of charge in the nonbonding regions, which together are the signature of the covalent bond.

In this paper, we apply our analysis to the standard deformation density for 1,2,7,8-tetraaza-4,5,10,11-tetraoxatricyclo[6.4.1.1]-tetradecane to explicate the unexpected features in this more complicated molecule. The calculation was performed on the full molecule in order to leave the substituent effects, long-range through-bond interactions, ring strain effects, and steric and electronic factors intact. Using the concept of a valence-state atom, we partition our theoretical deformation density into two electron-density differences so that one sees the origin of all of the unexpected features. Lastly, we address the subject of whether the standard deformation density and/or our partitioning schemes have the potential to indicate the relative strength of various bonds.

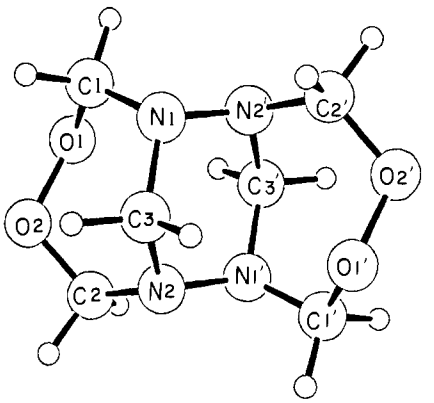

Figure 1. Geometry of 1,2,7,8-tetraaza-4,5,10,11-tetraoxatricyclo-[6.4.1.1]tetradecane generated from the supplemental material of atomic coordinates and unit cell parameters from the X-ray crystal structure reported by Dunitz and Seiler.[4a] The atoms are arbitrary sizes. The molecule has only a center of inversion. The C–O–O–C dihedral angle is 100° and the X–N–X bond angles are approximately 115°.

Computational Procedure

The molecular and atomic orbitals were generated by ab initio calculations using as basis functions the standard Dunning double-ζ [4s2p] contraction[23a] of the Huzinaga (9s5p) primitive Gaussian basis.[23b] Orbitals for the molecule were generated by calculations at the single-determinant Hartree–Fock–Roothaan (HFR) level.[24] Gross atomic charges were calculated from total atomic orbital Mulliken populations. The canonical HFR molecular valence orbitals, which are delocalized over the entire molecule, were localized using Boys' criteria[25] to generate orbitals for the individual bonding orbital densities and lone-pair orbital densities. The localization of the molecular orbitals is an orthonormal transformation and does not change the total energy or the total electron density distribution. The atomic hybridization,[26] atomic orbital populations, and overlap populations of each LMO were evaluated.

Atomic orbitals were generated by calculations in the same basis at the symmetry equivalenced restricted Hartree–Fock–Roothaan (SERHF) level.[27] Hybrid valence atomic orbitals for each atom were generated from the localized molecular orbitals (LMO) by truncation of the functions on the other atom.[28] Atomic core orbitals and hybrid atomic valence orbitals were then renormalized and symmetrically orthogonalized using the Lowdin procedure.[29] The energy of the resulting hybrid atom was determined. All of the above were performed with the ATMOL3 system of programs.[30]

The various wave functions with the appropriate electron occupation numbers were used in the program MOPLOT[31] to generate total electron density maps and bonding orbital and lone-pair orbital electron density maps for the molecule and for the atoms. All the occupied molecular orbitals contain two electrons. For the spherical atoms, the $2p_x$, $2p_y$, and $2p_z$ orbitals for the O, N, and C atoms are occupied by 4/3 electron, 1 electron, and 2/3 electron, respectively. For the hybrid atoms, the atomic hybrid orbitals used for bonding are singly occupied and the lone-pair atomic hybrid orbitals doubly occupied. Density difference maps were

(15) Bader, R. F. W.; Henneker, W. H.; Cade, P. E. *J. Chem. Phys.* **1967**, *46*, 3341.
(16) Bader, R. F. W.; Beddall, P. M. *J. Chem. Phys.* **1972**, *56*, 3320.
(17) (a) Bader, R. F. W.; Keaveny, I.; Cade, P. E. *J. Chem. Phys.* **1967**, *47*, 3381. (b) Bader, R. F. W.; Bandrauk, A. D. *Ibid.* **1968**, *49*, 1653. (c) Cade, P. E.; Bader, R. F. W.; Henneker, W. H.; Keaveny, I. *Ibid.* **1969**, *50*, 5313.
(18) (a) Bader, R. F. W. *Acc. Chem. Res.* **1985**, *18*, 9. (b) Bader, R. F. W.; MacDougall, P. J.; Lau, C. D. H. *J. Am. Chem. Soc.* **1984**, *106*, 1594. (c) Bader, R. F. W.; Essen, H. *J. Chem. Phys.* **1984**, *80*, 1943. (d) Bader, R. F. W.; Nguyen-Dang, T. T.; Tal, Y. *Rep. Prog. Phys.* **1981**, *44*, 893.
(19) (a) Cremer, D.; Kraka, E. *Croat. Chem. Acta* **1984**, *57*, 1259. (b) Cremer, D.; Kraka, E. *Angew. Chem., Int. Ed. Engl.* **1984**, *23*, 627.
(20) Kunze, K. L.; Hall, M. B. *J. Am. Chem. Soc.* **1986**, *108*, 5122.
(21) (a) Schwarz, W. H. E.; Valtazanos, P.; Ruedenberg, K. *Theor. Chim. Acta* **1985**, *68*, 471. (b) Schwarz, W. H. E.; Mensching, L.; Valtazamos, P.; von Niesson, W. *Int. J. Quantum Chem.* **1986**, *14*, 909.
(22) Hirshfeld, F. L., to be published.
(23) (a) Dunning, T. H., Jr. *J. Chem. Phys.* **1970**, *53*, 2823. (b) Huzinaga, S. *Ibid.* **1965**, *42*, 1293.
(24) Roothaan, C. C. J. *Rev. Mod. Phys.* **1951**, *23*, 69.
(25) Foster, J. M.; Boys, S. F. *Rev. Mod. Phys.* **1960**, *32*, 300.
(26) Newton, M. D.; Switkes, E. *J. Chem. Phys.* **1971**, *54*, 3719.
(27) Guest, M. F.; Saunders, V. R. *Mol. Phys.* **1974**, *28*, 819.
(28) (a) A somewhat related method was developed by Newton et al. (Newton, M. D.; Switkes, E.; Lipscomb, W. N. *J. Chem. Phys.* **1970**, *53*, 2645), who transformed canonical SCF orbitals to "localized" (LMO) form by the Edmiston–Ruedenberg procedure (*Rev. Mod. Phys.* **1963**, *35*, 457) and then extracted the portion of each LMO belonging to the central atom as the appropriate hybrid.
(29) Lowdin, P.-O. *J. Chem. Phys.* **1950**, *18*, 365.
(30) Hillier, I. H.; Saunders, V. R.; Guest, M. F. ATMOL3 System, Chemistry Department, University of Manchester, Manchester, U.K., and SERC Laboratory, Daresbury, U.K.
(31) Lichtenberger, D. L. Ph.D. Dissertation, University of Wisconsin, Madison, WI, 1974. Program available from: Quantum Chemistry Program Exchange, Indiana University, Bloomington, IN 47401; Program 284.

generated by subtraction of one total map from another. The isolated individual orbital density difference maps were generated by subtraction of the atomic orbital density map from the molecular orbital density map. All of the above calculations were performed on the Texas A&M University Chemistry Department VAX 11/780 computer.

Maps with contours of constant density difference were plotted on a Xerox 9700 Electronic Printing System with the graphics package called Electronic Printer Image Construction (EPIC) using the program CONTOUR[32] on the Texas A&M University Amdahl 470V/7 and V/8 computers. In the contour line diagrams, solid lines represent positive density difference and dashed lines represent negative difference. The smallest positive and negative contours are ±0.075 electron Å^{-3} and adjacent contours of the same sign differ by an increment of 0.075 electron Å^{-3} in all maps.

Geometry

The geometry of this centrosymmetric molecule is shown in Figure 1 and was calculated directly from the atomic coordinates of the X-ray crystal structure reported by Dunitz and Seiler.[4a] C–H bonds are typically 1.08 to 1.10 Å; Dunitz and Seiler displaced the H from their refined positions along the appropriate C–H directions to a C–H distance of 1.08 Å. The central tetraazacyclohexane ring has the chair conformation with the N lone-pair directions equatorial. Note that the C–O–O–C dihedral angle is 100°, similar to that of 102° in peroxide which would not be possible with a six-membered ring. The C3–N1–C1–O1 dihedral angle is 58°, while the C3–N2–C2–O2 dihedral angle is 14.5°. Thus, the lone-pair direction at N1 is antiperiplanar to the C1–O1 bond while the lone-pair direction at N2 is anticlinal to the C2–O2 bond. There is a slight difference between the N1–C1 and N2–C2 bond lengths and between the O1–C1 and O2–C2 bond lengths. The X–N–X bond angles are approximately 115°.

Molecular Orbital Analysis of the Electronic Structure and Bonding

The optimum hybridization of an atom in a molecule has an intrinsic existence which depends on the number of electrons in the valence shell and on the energy difference between the 2s and 2p orbitals.[33] This competes with the Pauli exclusion principle which always favors canonical sp^3 hybrids for atoms such as C, N, and O.[34] When hybridization mixes 2s character into a singly occupied 2p σ-bonding orbital, the doubly occupied 2s loses electron density and the 2p σ-bonding orbital gains electron density in order to move the doubly-occupied, nonbonding 2s out of the bonding region. Since it is more stable to doubly occupy the predominantly 2s hybrid than the predominately 2p hybrid, the mainly 2s lone-pair hybrid points away from the bond center and contains two electrons, while the mainly 2pσ bonding hybrid points toward the bond center and contains only one electron. Thus, as two atoms bond, hybridization reduces but does not eliminate nonbonded repulsions of the lone pairs.

Since the average difference in energy of the 2s and 2p orbitals[35] and the number of valence electrons vary with the atom, the degree of intrinsic hybridization varies with the different atoms. Thus in the absence of additional forces, there is more hybridization in C than in N and more in N than in O, consistent with the 2s–2p promotion energies. Since the promotion energy is relatively large for the O atom,[35] the degree of intrinsic hybridization is small.

The degree that ring strain modifies the intrinsic hybridization depends on the 2s–2p promotion energies. The O–O dihedral angle of 100° in this molecule is close to that of 102° in peroxide because it depends predominantly on the intrinsic hybridization of the O atom. Our analysis of the hybridization of the LMO's based on population analysis shows the O hybrid orbitals in the O–O and C–O bonds to have more 2p (sp$^{4.3}$ and sp$^{2.7}$, respectively) than the lone-pair orbitals (sp$^{1.8}$). However, the N lone pair is hybridized with more 2p character than the bonding atomic orbitals on N. Our analysis of the LMO's shows the N bonding atomic orbital in the N–N bond to have sp$^{2.1}$, that in the C–N bonds to have sp$^{1.5}$, and the N lone-pair hybrid orbital to have sp$^{2.9}$. Thus, the modification of hybridization due to strain has occurred at N (X–N–X angles approximately 115°) instead of O since it is easier to promote N than O. Not unexpectedly our analysis of the LMO's shows the C hybrid orbitals to be equally hybridized for all four bonds, but as is typical of this analysis they appear to have a hybridization closer to sp^2 than the ideal sp^3.

Comparison of Computational and Experimental Aspects of Standard Deformation Density Determinations

There have been many studies comparing theoretical and experimental electron density distributions in order to check the reliability of both approaches.[7,36-47] Previous findings showed that the basis set error in theoretical molecular electron density distributions is pronounced and, especially, that the addition of polarization functions results in a small change in energy of the molecule, but a large change in electron density.[7,20,36] In general, the basis set used for this calculation will be responsible for under-estimating the electron density in the bonding regions and overestimating it in the lone-pair regions. The addition of electron correlation (CI) would result in a large change in the energy of the molecule, but only a small change in the electron density near the internuclear region.[7,13a,20] Although calculations in larger basis sets or including CI may modify the actual magnitude of the density features, they should not alter the qualitative aspects, which we emphasis here. Although there is a possibility of systematic error due to the details of the experiment and refinement procedure,[6,48] a carefully done study of a light-atom, centrosymmeteric structure such as that of Dunitz and Seiler should be fairly reliable. However, it will differ from the usual theoretical density because of thermal motion. In order to directly and quantitatively compare experimental and theoretical electron density distributions, one would take into account the effect of this thermal smearing of the experimental density by incorporation of it into the theoretical maps or by the production of static experimental maps.[49-52] Since correction of the static theoretical maps for thermal motion leaves the main features of the maps unchanged and simply reduces the height of the peaks and broadens troughs throughout the maps, we will simply use our static maps in this qualitative comparison.

Standard Deformation Density

Subtraction of the superposition of spherically averaged atomic densities from the molecular density results in the theoretical standard deformation density for 1,2,7,8-tetraaza-4,5,10,11-tetraoxatricyclo[6.4.1.1]tetradecane, for which contour maps of several planes through it are shown in Figure 2. The corresponding experimental maps of Dunitz and Seiler[4a] are reproduced in Figure 3. The qualitative agreement is excellent. All of the unexpected features are seen in both maps.

(32) An in-house program that uses CONREC a special smoothing routine for drawing contours, developed at the National Center for Atmospheric Research (NCAR), Boulder, Co., and adapted for use on the Amdahl 470V/6 by Thomas Reid, Data Processing Center, Texas A&M University.

(33) (a) Hall, M. B. *J. Am. Chem.* Soc. **1978**, *100*, 4333. (b) Hall, M. B. *Inorg. Chem.* **1978**, *17*, 2261.
(34) Lennard-Jones, J. E. *J. Chem. Phys.* **1952**, *20*, 1024.
(35) Murrell, J. N.; Kettle, S. F. A.; Tedder, J. M. *Valence Theory*, 2nd ed.; Wiley: New York, 1970; p 34.
(36) Hall, M. B. In ref 1, Chapter 4.1.
(37) Kok, R. A.; Hall, M. B. *J. Am. Chem. Soc.* **1985**, *107*, 2599.
(38) Ruysink, A. F. J.; Vos, A. *Acta Crystallogr., Sect. A* **1974**, *30*, 497.
(39) Bats, J. W.; Feil, D. *Chem. Phys.* **1977**, *22*, 175.
(40) DeWith, G. *Chem. Phys.* **1978**, *32*, 11.
(41) Benard, M. *J. Am. Chem. Soc.* **1978**, *100*, 7740.
(42) Stevens, E. D. *Acta Crystallogr., Sect. B* **1980**, *36*, 1876.
(43) Benard, M.; Coppens, P.; DeLucia, M. L.; Stevens, E. D. *Inorg. Chem.* **1980**, *19*, 1924.
(44) Mitschler, A.; Rees, B.; Wiest, R.; Benard, M. *J. Am. Chem. Soc.* **1982**, *104*, 7501.
(45) Heijser, W.; Baerends, E. J.; Ros, P. *Symp. Faraday Soc.* **1980**, *14*, 211.
(46) Leung, P. C.; Coppens, P. *Acta Crystallogr., Sect. B* **1983**, *39*, 535.
(47) Kutzler, F. W.; Swepston, P. N.; Berkovitch-Yellin, Z.; Ellis, D. E.; Ibers, J. A. *J. Am. Chem. Soc.* **1983**, *105*, 2296.
(48) Stevens, E. D., Coppens, P. *Acta Crystallogr., Sect. B* **1980**, *36*, 1864.
(49) Hase, H.; Reitz, H.; Schweig, A. *Chem. Phys. Lett.* **1976**, *39*, 157.
(50) Coppens, P.; Stevens, E. D. *Isr. J. Chem.* **1977**, *16*, 175.
(51) Stevens, E. D.; Rys, J.; Coppens, P. *Acta Crystallogr., Sect. A.* **1977**, *33*, 333.
(52) Coppens, P. In ref 1, Chapter 1.2.

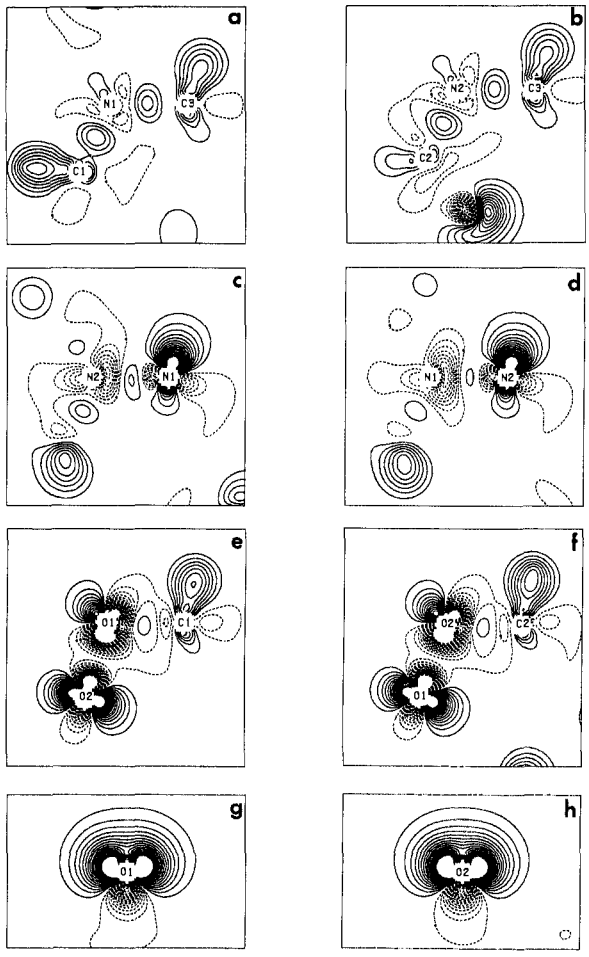

Figure 2. Contour plots of several planes through the theoretical standard deformation density, molecular density minus density of spherically averaged atoms. The planes are as follows: (a) through C1, N1, and C3; (b) through C2, N2, and C3; (c) through N2′, N1, and the midpoint of C1 and C3; (d) through N1′, N2, and the midpoint of C2 and C3; (e) containing O2, O1, and C1; (f) containing O1, O2, and C2; (g) perpendicular to (e) and passes through O1 and the midpoint of O2 and C1; and (h) perpendicular to (f) and passes through O2 and the midpoint of O1 and C2. For all plots in this paper, positive contours are solid, negative contours are dashed, and the zero contour is omitted. Adjacent contours differ by an increment of 0.075 electron Å^{-3}. The smallest contour is ±0.075 electron Å^{-3}.

C–N Single Bonds. Only weak bonding density accumulations are found at the centers of the C–N covalent single bonds (plane a through C1, N1, and C3, and plane b through C2, N2, and C3). There is a trough of density deficit in the interatomic regions near the N nucleus. In our theoretical maps there is accumulation around the carbon, which is not seen in the experimental maps, perhaps, because it is close to the nucleus. This pattern of gain of density around the carbon and loss of density around the nitrogen is opposite in direction to that of the charge transfer which is expected based on electronegativity arguments.

N–N Single Bond and N Lone Pair. The standard deformation density of the N–N single bonds are shown in plane c through N2′, N1, and the midpoint of C1 and C3, and plane d through N1′, N2, and the midpoint of C2 and C3. It is mostly negative in the internuclear region with a very weak accumulation of charge in the center with deep troughs of density deficit nearer the nuclei. This density pattern is typical of standard deformation densities of N–N single bonds.[10] On N1 in map c and N2 in map d is seen significant buildup of electron density, which peaks at about 0.4 Å on one side of the N perpendicular to the N–N bond, with a secondary lobe opposite it. The centroid of the LMO representing this lone pair is 0.35 Å from the nucleus. Dunitz and Seiler correctly interpret the main peak to be the approximately tetrahedrally oriented N lone pair. The second lobe is not typical of

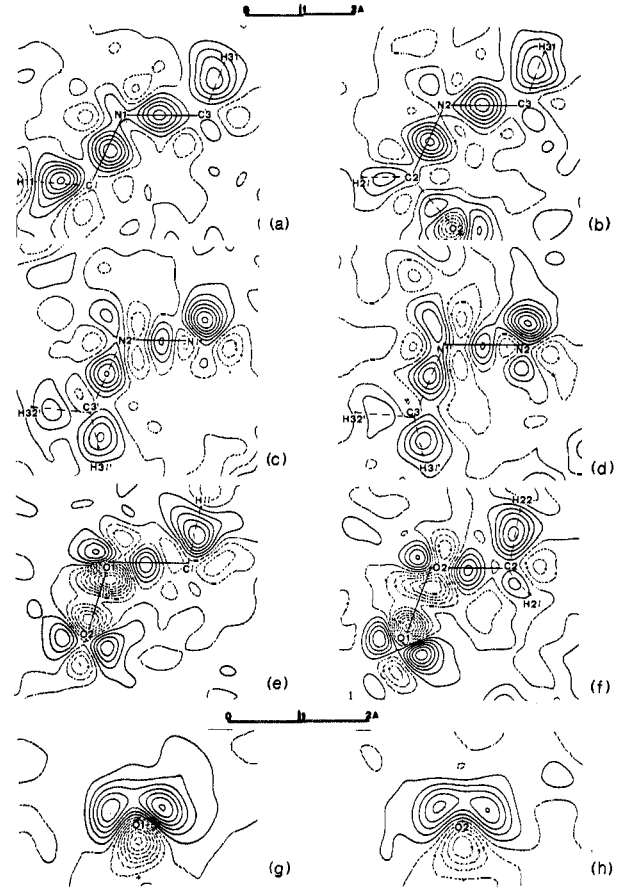

Figure 3. Reproduction of contour maps of same planes as in Figure 2 from Dunitz and Seiler's experimental standard deformation density. The planes and contour intervals are the same as in Figure 2.

standard deformation densities of N lone pairs.[36,53]

C–O and O–O Single Bonds. Maps for the C–O and O–O single bonds are in plane e containing O2, O1, and C1, and plane f containing O1, O2, and C2. For the O–O bond the maps show an electron density deficit along the bond axis throughout the internuclear bonding region and beyond the nuclear centers with deep troughs near the atoms and a more shallow deficit in the center. In this plane, which bisects the lone pairs, we also see density buildup at each O atom in the π regions perpendicular to the O–O bond axis. This is typical of standard deformation densities of O–O bonds.[6,7] For the C–O bonds only weak bonding density accumulations are found in the centers of the bonds with troughs of density deficit in the interatomic regions near the O nuclei. In our theoretical maps there is accumulation near the carbon in these C–O bonds but, again, not in the experimental maps, possibly due to factors mentioned above for the C–N bonds. Again, this pattern of gain of density around the carbon and loss of density around the oxygen is opposite in direction to the expected charge transfer, but is typical of standard deformation densities of C–O bonds.[9]

O Lone Pairs. The map in plane g is perpendicular to plane e and passes through O1 and the midpoint of O2 and C1. The map in plane h is perpendicular to plane f and passes through O2 and the midpoint of O1 and C2. These maps show strong bilobed accumulations of density which peak at about 0.4 Å from the O atoms and make an angle of about 120–130°. The LMO centroids for these lone pairs occur at 0.32 Å. Dunitz and Seiler correctly interpret these to be approximately tetrahedrally oriented O lone pairs. These are typical of the O lone pairs in peroxides.[6,7]

Thus, the accumulation of density in the various bonds is less than that in the O and N lone-pair peaks and decreases in the order C–N > C–O > N–N > O–O. The weak bonding density

(53) Irngartinger, M. In ref 1, Chapter 5.5.

accumulations and deficits and some patterns of gain and loss of density seem at variance with our intuition. The strong resemblance of the experimental and theoretical deformation density in these covalent bonds suggests that the problem lies with our intuition. Although the analysis of electron difference densities based on a promolecule of spherical atoms is experimentally quite appealing, it may not be the most appropriate reference density for a discussion of the bonding. The unexpected features are explicable, as we will show.

Analysis of Standard Deformation Density

Spherical C Atom. Each spherical $2s^22p^2$ C atom is a linear combination of all components of the spectroscopic ^3P ground state of the atom, each of which has two singly occupied 2p orbitals. Thus the $2p_x$, $2p_y$, and $2p_z$ orbitals are, on the average, each occupied by 2/3 electron. The promoted $2s^12p^3$ ^5S state atom is spherical and has the same density as the canonical sp^3 hybrid atom, and it differs little in density from that of the spherically averaged ^3P ground state since the maxima in the radial distributions of the electron density of the 2s and 2p orbitals occur at about the same distance from the nucleus and the hybrids are equally occupied. Apparently the use of spherical ^3P ground-state C atoms has not led to an interpretation problem. However, a closer look at the radial distribution of the electron density of the orbitals shows that the 2p, which is less than singly occupied in the spherical atom, dominates at distances closer to the nucleus where the doubly occupied 2s has a node. As can be seen in Figure 2a–d, use of the ground-state C atom in the promolecule results in an accumulation of density seen around the C atom in the C–O and C–N bonds. Thus, these features in the standard deformation density of the C–O and C–N bonds result, in part, from promotion of the C atom.

Spherical N Atom. Since the spherical ground-state $2s^22p^3$ N atom is the only component of the spectroscopic ^4S ground state, atomic orientation is ordinarily not a major problem. However, in forming bonds the N atom hybridizes, which moves the doubly occupied lone pair away from the bonding region and results in atomic hybrids which are unequally occupied, i.e., singly occupied bonding hybrids and doubly occupied lone pair hybrids. Thus, the N–N and C–N bonds appear weak because of the subtraction of the density of the doubly occupied N 2s atomic orbitals from the density of the two-electron bonding molecular orbitals. This removal of electron density causes pronounced troughs near the N atoms in the N–N bonds and in the C–N bonds. Likewise, fewer electrons are removed from the doubly occupied N lone-pair molecular orbital, due to the subtraction of singly occupied 2p atomic orbitals. This results in a standard deformation density with density excess for the lone pair. Thus, the loss of density near the N and accumulation near the C in the C–N bonds are not due to electronegativity differences. The deformation density around N appears somewhat different from other N atoms because of the strain, which results in more 2p character and less 2s character in the lone pair than is usual. The density for the lone pair appears as a main peak with a secondary lobe on the other side. Thus, the features in the N–N and C–N bonds include promotion of both N and C and N lone-pair density from polarization and hybridization.

Spherical O Atom. Each spherical ground-state $2s^22p^4$ O atom is a linear combination of all components of the spectroscopic ^3P ground state of the atom, each of which has one doubly occupied and two singly occupied 2p orbitals. Thus, the $2p_x$, $2p_y$, and $2p_z$ orbitals are, on the average, each occupied by 4/3 electron. Although one component has the same energy as the other components, inclusion of all components in the spherical atom also includes those components that would contribute predominantly to antibonding excited states of the molecule. Although it is a convenient reference density, it is not appropriate for a discussion of the bonding, since atomic bonding orbitals must be singly occupied for the pairing of electrons to occur during covalent bonding. For the C–O bond this results in only a weak density buildup. For the O–O bond this more than compensates for the constructive interference, resulting in a negative deformation density. Since the mostly $2p\sigma$ O–O bonding molecular orbital extends beyond the nuclei along the bond axis, subtraction of the more than singly occupied atomic 2p orbitals results in a negative deformation density there also. Compared to the doubly occupied O lone-pair molecular orbitals, fewer electrons are removed via the less than doubly occupied 2p atomic orbitals, resulting in excess density accumulations in the lone-pair regions in Figure 2g,h and density accumulations at each O atom perpendicular to the O–O bond axis in Figure 2e,f.

Hybrid-Atom Deformation Density

Since the changes in the atomic orientation of the O atoms and the promotion, polarization, and hybridization of all the atoms cause interpretation problems and even mask more subtle changes due to constructive interference and charge transfer, it would be helpful to have an intermediate density which separates these effects. A meaningful intermediate density can be constructed from the electron densities of valence-state hybrid atoms, which preserve the orientation, promotion, and hybridization of the atoms in the molecule. The valence-state deformation density is defined as the change in density due to covalent bond formation from the valence-state hybrid atoms and was calculated as the difference in density between the molecule and the valence-state hybrid atoms. The atomic density difference is defined as the change in density due to the preparation of atoms for bonding by orientation of the ground-state ^3P O atoms and then promotion, polarization, and hybridization of all atoms prior to molecular formation, and was calculated as the difference in density between the valence-state hybrid atoms and the spherically averaged ground-state atoms.

Subtraction of the electron densities of optimally hybridized valence-state atoms has matched the lone-pair densities of atoms and molecule so that the total difference is dominated by bonding density differences. Although this is complicated owing to the many bonds, the primary features of one bond in the total density difference can be isolated and reduced to that of a two-electron localized bonding molecular orbital density difference. This is calculated as the density difference between the localized two-electron bonding molecular orbital and the corresponding two singly occupied valence-state atomic hybrid orbitals. Density must flow from the nonbonding regions to the bonding region for there to be a density buildup between the nuclei, since the total density is constant. The analogous lone-pair orbital density differences are almost featureless.

Since there are strong similarities between pairs of planes (i.e., planes a and b) shown in Figures 2 and 3, in the following results and discussion we will only show the results for one of the two planes; thus, we will examine planes b, d, f, and h of Figures 2 and 3.

C–N Single Bonds. Partitioning the standard deformation density containing the C–N bonds in Figure 2b results in the atomic density difference, Figure 4b1, due to preparation of atoms for bonding, and the valence-state deformation density, Figure 4b2, due to covalent bond formation. The standard formation density, Figures 2b, is the sum of these two densities (Figure 4b1 plus Figure 4b2). The features due to covalent bond formation of the individual C–N bonds in Figure 4b2 are isolated to two-electron density differences, seen in Figure 4, b3 and b4. The deformation density of covalent bond formation show strong density accumulations in the internuclear regions which are shifted away from the carbon toward the nitrogen with loss of density around the carbon and gain around the nitrogen. The average gross atomic charges of +0.07 and −0.35 and the average atomic populations of the LMOs of 0.64 and 0.43 for C and N, respectively, indicate charge transfer from C to N. Thus, these maps show both constructive interference of covalent bond formation and charge transfer in the C–N bonds.

The deformation density due to preparation of the atoms for bonding show density deficit in the internuclear region near N with loss of density around the nitrogen and accumulation around the carbon, as found in the standard deformation density of these C–N bonds. Because the resulting hybrids are unequally occupied

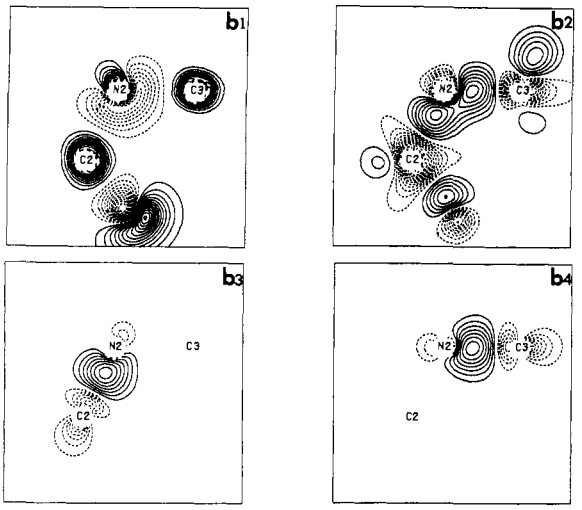

Figure 4. Plane b is shown for the atomic difference density, valence-state hybrid atoms minus spherical ground-state atoms (b1), for the valence-state deformation density, molecular density minus the density of valence-state hybrid atoms (b2), and for the two isolated localized orbital deformation densities, two-electron orbital density minus two one-electron densities from each atomic hybrid orbital (b3 and b4). The contour intervals are the same as those in Figure 2.

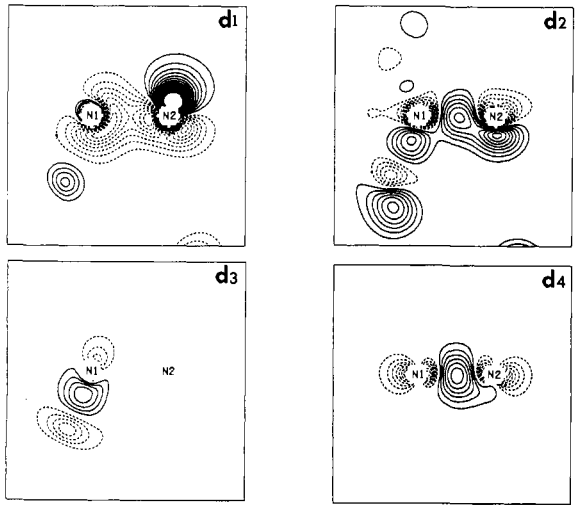

Figure 5. Plane d is shown with a set of maps similar to those in Figure 4. Plot d1 is the atomic difference density, plot d2 is the valence-state deformation density, and plots d3 and d4 are the localized orbital density differences. The contour intervals are the same as those in Figure 2.

in N, this atom promotion, polarization, and hybridization corresponds to a relatively strong charge displacement from the bonding region near the N nucleus to the lone-pair region which is approximately perpendicular to this plane. This is not seen in C because the C hybrids are equally occupied. Thus, these features in the standard deformation density are entirely due to the effects of promotion, polarization, and hybridization of the C and N atoms, in preparation for bonding.

N–N Single Bond and N Lone Pair. Partitioning the standard deformation density containing the N–N bond and the N lone pair in Figure 2d results in Figure 5d1 due to preparation of atoms for bonding, and Figure 5d2 due to covalent bond formation. The features due to covalent bond formation of the individual N–N bonds in Figure 5d2 are isolated to two-electron density differences, seen in Figures 5, d3 and d4. The maps of the density of covalent bond formation show strong accumulation of charge along the bond axis throughout the internuclear region. The lone-pair density accumulation with the secondary lobe opposite it have been matched by the prepared atom lone pair and are not seen. The deformation density due to preparation of atoms for bonding Figure 5d1 shows electron density deficit in the internuclear region with deep troughs of density deficit nearer the nuclei. Also seen

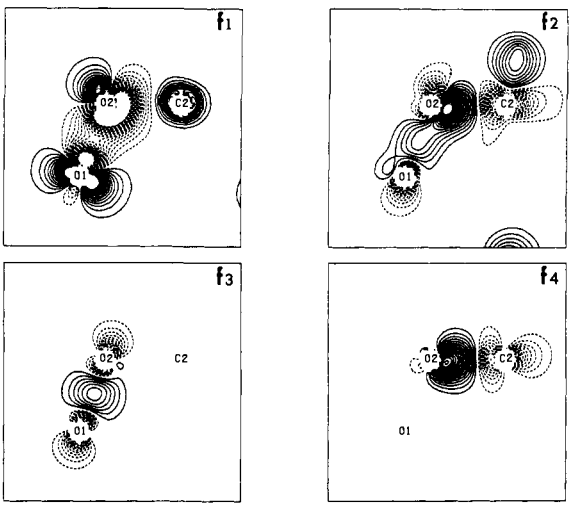

Figure 6. Plane f is shown with a set of maps similar to those in Figure 4. Plot f1 is the atomic difference density, plot f2 is the valence-state deformation density, and plots f3 and f4 are the localized orbital density differences. The contour intervals are the same as those in Figure 2.

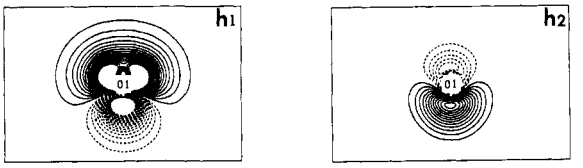

Figure 7. Plane h is shown for the atomic density differences (h1) and for the valence-state deformation density (h2). The contour intervals are the same as those in Figure 2.

is the N lone pair with electron density excess on one side of the N perpendicular to the N–N bond and with the secondary lobe on the other side. The atom promotion, polarization, and hybridization corresponds to a relatively strong charge displacement from the bonding region near the N nuclei to the lone-pair regions in this plane because the resulting hybrids are unequally occupied. Thus, these latter features in the standard deformation density are entirely due to the effect of promotion and lone-pair polarization and hybridization in preparation for bonding.

C–O and O–O Single Bonds. Partitioning the standard deformation density containing the C–O and O–O bonds in Figure 2f results in Figure 6f1 due to preparation of atoms for bonding, and in Figures 6f2 due to covalent bond formation. The features due to covalent bond formation of the individual O–O and C–O bonds in Figures 6f2 are isolated to two-electron density differences, seen in Figures 6, f3 and f4. For the O–O bonds, the deformation density of covalent bond formation reveal strong electron density accumulation along the bond axis throughout the internuclear bonding region, due to constructive interference, with density deficits beyond the nuclear centers along the bond axis. This is what one would expect for bonding between orbitals which are predominantly p in character.

For the C–O bonds strong density accumulation is found in the internuclear region which is greatly shifted away from the carbon toward the oxygen with loss of density around the carbon and gain around the oxygen. The average gross atomic charges of +0.07 and −0.31 and the atomic populations of the LMOs of 0.34 and 0.71 for C and O, respectively, indicate charge transfer with more O character than C character in the LMO. Here, the charge transfer in the C–O bond is greater than that in the C–N bonds and almost completely masks the constructive interference of covalent bond formation.

O Lone Pairs. Partitioning the standard deformation density containing the O lone pairs in Figure 2h results in Figure 7h1 due to preparation of atoms for bonding and Figure 7h2 due to covalent bond formation. The maps of the density of covalent bond formation show that we have matched the density in the lone-pair regions such that we see density deficits on the lone pair of the

O atom due to charge transfer.

Conclusion

From the large electron density deficit between the oxygens and the weak electron density accumulation in the centers of the N-N, C-O, and C-N bonds and other features in the standard deformation density for 1,2,7,8-tetraaza-4,5,10,11-tetraoxatricyclo[6.4.1.1]tetradecane, one might infer that there might be deficiencies in the theory of covalent bonds. However, the features are due to the choice of a spherical-atom promolecule. Although the spherical-atom promolecule has important advantage for the experimentalist, all partitioning schemes, ours included, are arbitrary. However, the standard deformation density can be difficult to interpret without some additional "tools". To begin with, for electronegative atoms with more than half-filled shells, such as oxygen, the changes in the electron density due to the formation of the O-O single chemical bond are masked by the atomic orientation of O in the promolecule. Here, orientation of the O atoms in the promolecule improves the situation, and is particularly important because it has a dramatic effect on the density difference but does not change the energy.

The subtraction of any promolecule is useful only if it reveals features related to chemical concepts that are not visible in the total density. Here we have revealed features which are meaningful for chemists by using the chemical concept of a valence-state atom. We have partitioned the standard deformation density for this molecule into two parts corresponding to the often dominant change in density in preparation for bonding (atomic orientation of ground-state spherical O atoms and then promotion, polarization, and hybridization of all the atoms) and the smaller change in density due to covalent bond formation (constructive interference and charge transfer between valence-state optimum hybrids). Also, using these "prepared-for-bonding atoms", we isolated each bond from the complex difference density as a difference density of the two-electron bond. For the O-O and N-N bonds, the difference densities of covalent bond formation reveal not only the strong accumulation of charge in the internuclear region but also the concomitant depletion of charge in the nonbonding regions beyond the nuclear centers along the bond axis which together are the signature of the covalent bond. For the C-O and C-N bonds, similar maps show the correct direction of loss and gain of density due to charge transfer in these polar covalent bonds. The N is atypical because the strain causes the lone pair to contain more p character than an unstrained lone pair.

Thus, the unexpected features are explicable. One easily sees why the electron density in covalent bonds may appear weak or absent and why the patterns of gain and loss of density appear opposite that expected when two spherical atoms form a bond. The standard deformation densities of C-C and C-H bonds in typical organic molecules show quite large accumulations of density, since the density of the usual spherical atom reference is much closer to that of the valence state for C and H than it is for atoms which have lone pairs like O and N.

Is there a relationship between the standard deformation density of a bond and the strength of the bond? No, not even qualitatively. Is there a choice of promolecule for which there would be a simple direct relationship? A promolecule made from simple oriented ground-state atoms would not work since hybridizations and especially charge transfer can mask the constructive interference. For different bonds, the deformation density is not proportional to bond strength. Our partitioning scheme has potential, but is limited because even here charge transfer can mask constructive interference.

Acknowledgment. The authors gratefully acknowledge the support of the National Science Foundation. Grant No. CHE 83-09936 and CHE 86-19420 supported this work and Grant No. CHE 80-15792 assisted in the purchase of the VAX 11/780.

Registry No. 1,2,7,8-Tetraaza-4,5,10,11-tetraoxatricyclo[6.4.1.1]tetradecane, 81286-97-7.

Acid-Catalyzed Hydrogenation of Olefins. A Theoretical Study of the HF- and H_3O^+-Catalyzed Hydrogenation of Ethylene

Juan Carlos Siria, Miquel Duran, Agusti Lledós, and Juan Bertrán*

Contribution from the Departament de Quimica, Universitat Autònoma de Barcelona, 08193 Bellaterra, Catalonia, Spain. *Received March 11, 1987*

Abstract: The HF- and H_3O^+-catalyzed hydrogenation of ethylene and the direct addition of molecular hydrogen to ethylene have been studied theoretically by means of ab initio MO calculations using different levels of theory. The main results are that catalysis by HF lowers the potential energy barrier to a large extent, while catalysis by H_3O^+ diminishes dramatically the barrier for the reaction. Entropic contributions leave these results unchanged. The mechanisms of the two acid-catalyzed hydrogenations are somewhat different. While catalysis by HF exhibits bifunctional characteristics, catalysis by H_3O^+ proceeds via an initial formation of a carbocation. It is shown that catalysis by strong acids may be an alternate way for olefin hydrogenation.

Both hydrogenation of olefins and dehydrogenation of alkanes are reactions of great industrial importance. The molecular addition of hydrogen to ethylene is a prototype of these reactions, which is known to occur via a high-energy barrier. It has been established for a long time that the reaction proceeding via a least-motion path with a four-centered transition state is symmetry forbidden.[1] Moreover, recent theoretical calculations have shown that the barrier for a reduced symmetry path is also very high.[2] It is thus not surprising that catalysis of this reaction has been a matter of great importance in the literature.

Since the turn of the 19th century, several metal catalysts have been used successfully at different pressures and temperatures.[3]

(1) Woodward, R. B.; Hoffmann, R. *The Conservation of Orbital Symmetry*; Verlag Chemie: Weinheim, 1970.

(2) Gordon, M. S.; Truong, T. N.; Pople, J. A. *Chem. Phys. Lett.* **1986**, *130*, 245-248.

(3) Augustine, R. L. *Catalytic Hydrogenation*; Marcel Dekker: New York, 1965.

0002-7863/87/1509-7623$01.50/0